

Conductance Spectroscopy of Exfoliated Thin Flakes of $\text{Nb}_x\text{Bi}_2\text{Se}_3$

C. Kurter,^{*,†,‡,§} A. D. K. Finck,^{‡,⊥} E. D. Huemiller,[‡] J. Medvedeva,[†] A. Weis,[‡] J. M. Atkinson,[‡] Y. Qiu,[†] L. Shen,[†] S. H. Lee,[†] T. Vojta,[†] P. Ghaemi,^{§,||} Y. S. Hor,[†] and D. J. Van Harlingen[‡]

[†]Department of Physics and Materials Research Center, Missouri University of Science and Technology, Rolla, Missouri 65409, United States,

[‡]Department of Physics and Materials Research Laboratory, University of Illinois at Urbana–Champaign, Urbana, Illinois 61801, United States,

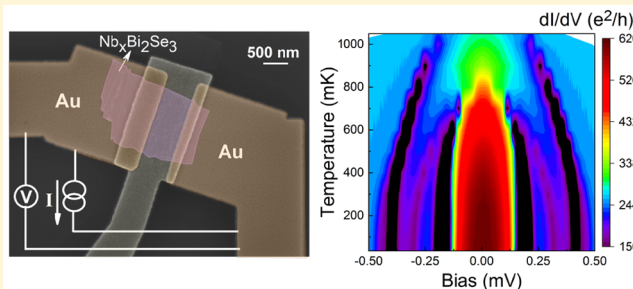
[§]Department of Physics, City College of New York of CUNY, New York, New York 10031, United States

^{||}Department of Physics, Graduate Center of CUNY, New York, New York 10016, United States

Supporting Information

ABSTRACT: We study unconventional superconductivity in exfoliated single crystals of a promising three-dimensional (3D) topological superconductor candidate, Nb-doped Bi_2Se_3 through differential conductance spectroscopy and magneto-transport. The strong anisotropy of the critical field along the out-of-plane direction suggests that the thin exfoliated flakes are in the quasi-2D limit. Normal metal-superconductor (NS) contacts with either high or low transparencies made by depositing gold leads onto Nb-doped Bi_2Se_3 flakes both show significant enhancement in zero bias conductance and coherence dips at the superconducting energy gap. Such behavior is inconsistent with conventional Blonder–Tinkham–Klapwijk theory. Instead, we discuss how our results are consistent with *p*-wave pairing symmetry, supporting the possibility of topological superconductivity in Nb-doped Bi_2Se_3 . Finally, we observe signatures of multiple superconducting energy gaps, which could originate from multiple Fermi surfaces reported earlier in bulk crystals.

KEYWORDS: Topological superconductivity, doped topological insulators, exfoliated $\text{Nb}_x\text{Bi}_2\text{Se}_3$, *p*-wave pairing symmetry, Andreev reflection spectroscopy, Majorana bound states



There has been tremendous effort to realize topological superconductivity in three-dimensional topological insulators either through proximity coupling to superconductors^{1–7} or through chemical dopants and intercalations.^{8–11} These superconductors are speculated to possess an unconventional superconducting gap with *p*-wave pairing symmetry^{12,13} that generally results in the formation of subgap surface Andreev bound states. Such exotic superconductors host zero energy Bogoliubov quasiparticles that mimic Majorana Fermions.^{14,15} Majorana modes have a great potential to implement topologically protected quantum computation.¹⁶

One common method to investigate an exotic superconductor is to perform Andreev reflection spectroscopy on a localized normal metal-superconductor (NS) junction.¹⁷ This method has been employed to study conductance spectra obtained with a gold contact on superconducting doped topological insulators such as $\text{Cu}_x\text{Bi}_2\text{Se}_3$. The robust zero bias peaks at low temperatures are attributed to zero energy surface bound states and *p*-wave pairing symmetry.⁹ These intriguing results stimulated further spectroscopic experiments. However, low-temperature scanning tunneling microscopy (STM) measurements exhibited contradictory results¹⁸ that were consistent with *s*-wave pairing. Recent nuclear magnetic

resonance experiments presented more conclusive findings by showing spontaneously broken spin-rotation symmetry in the hexagonal plane of the electron-doped topological insulator $\text{Cu}_{0.3}\text{Bi}_2\text{Se}_3$ in the superconducting state suggesting evidence for spin-triplet pairing and nematicity.¹⁹

The devices we study in this paper employ localized normal metal leads fabricated on top of thin flakes of Nb-doped topological insulator Bi_2Se_3 , $\text{Nb}_x\text{Bi}_2\text{Se}_3$. The material claimed to have coexistence of magnetic ordering and unusual superconductivity¹⁰ due to spontaneous time reversal symmetry breaking.^{20,21} Moreover, torque magnetometry measurements reported rotational symmetry breaking suggesting a nematic order in the superconducting ground state of $\text{Nb}_x\text{Bi}_2\text{Se}_3$, consistent with an E_u pairing symmetry.²² Complementary directional penetration depth measurements supported the presence of rotational symmetry breaking and a nodal superconducting energy gap.²³ Recent scanning tunneling microscopy (STM) studies have reported the

Received: July 19, 2018

Revised: November 17, 2018

Published: November 27, 2018

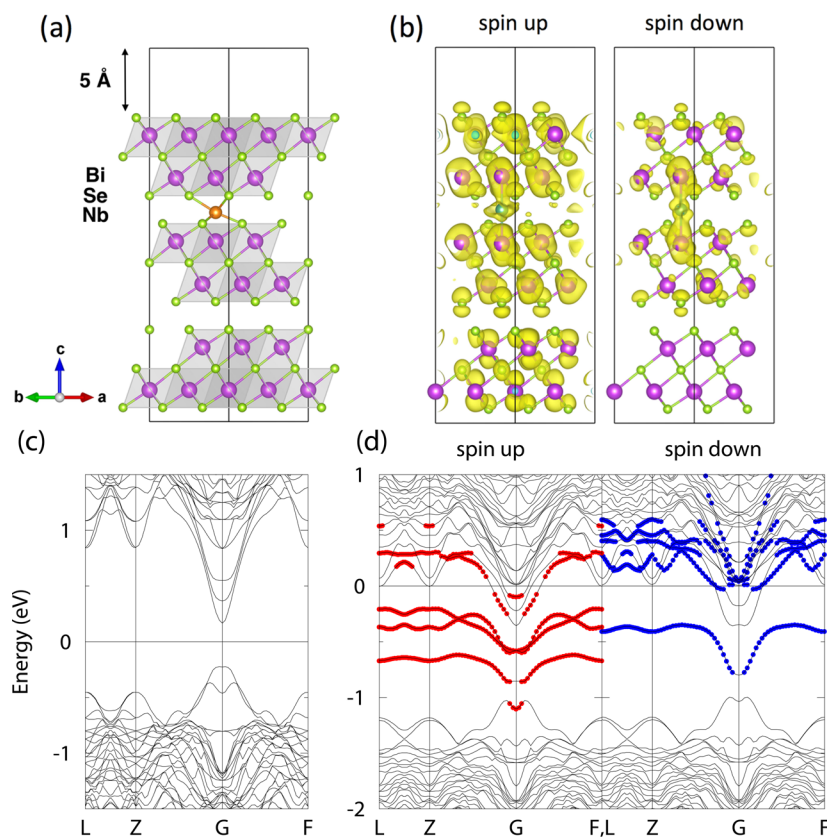


Figure 1. (a) The $\text{Nb}_x\text{Bi}_2\text{Se}_3$ slab used in the calculations showing quintuple layers of Bi_2Se_3 and single intercalated Nb atom. (b) The charge density distributions calculated within 20 meV below the Fermi level for $\text{Nb}_x\text{Bi}_2\text{Se}_3$. The charge isosurface level is the same for spin up and spin down electronic channels. (c,d) Calculated electronic structures of the Bi_2Se_3 slab and Nb doped Bi_2Se_3 slab for comparison.

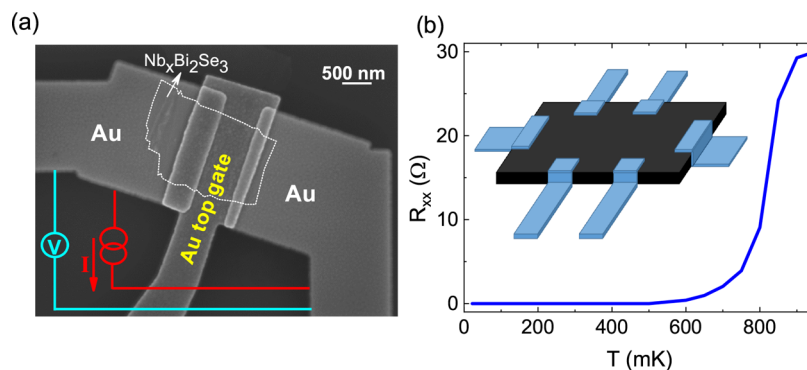


Figure 2. (a) Scanning electron microscopy image of a device, the conductance spectra of which is shown in Figure 3e,f, made with two gold leads on a 16 nm thick exfoliated piece of $\text{Nb}_{0.28}\text{Bi}_2\text{Se}_3$. The configuration of current and voltage probes for two-terminal measurements are schematically shown. (b) Longitudinal resistance as a function of temperature from a Hall bar device fabricated on a similar flake showing the transition temperature. Inset shows the schematics of the hall bar device.

existence of topological surface states²⁴ and supported the existence of unconventional superconductivity in $\text{Nb}_x\text{Bi}_2\text{Se}_3$.²⁵

Unlike the closest counterpart Cu doped Bi_2Se_3 , in $\text{Nb}_x\text{Bi}_2\text{Se}_3$ niobium intercalation leads to dramatic changes in the electronic band structure of Bi_2Se_3 partly because Nb with partially occupied d-states behaves as magnetic dopant and strongly interacts with hosting Bi_2Se_3 bands near the Fermi level.¹⁰ This leads to complex features in the Fermi surface associated with the material such as split states, new pockets, and significant difference between spin up and down electronic channels.²⁶ Contrary to Cu, Nb atom has a strong preference for the interconnect site as shown for the slab used in the

density functional theory (DFT) calculations that mimics our exfoliated thin crystals (Figure 1a). The strong hybridization between the d-state of a single Nb atom and quintuple layers of Bi_2Se_3 slab can be seen in the charge density distribution calculated within 20 meV below the Fermi level in Figure 1b, resolved for the spin up and down situations.

The calculated band structures of thin slabs of Bi_2Se_3 and Nb doped Bi_2Se_3 are shown in Figure 1c,d, respectively, for comparison. The details of the DFT calculations can be found in the Supporting Information. A single Nb atom intercalation modifies the band structure significantly. In particular, DFT calculations show that electronic bands with different spin

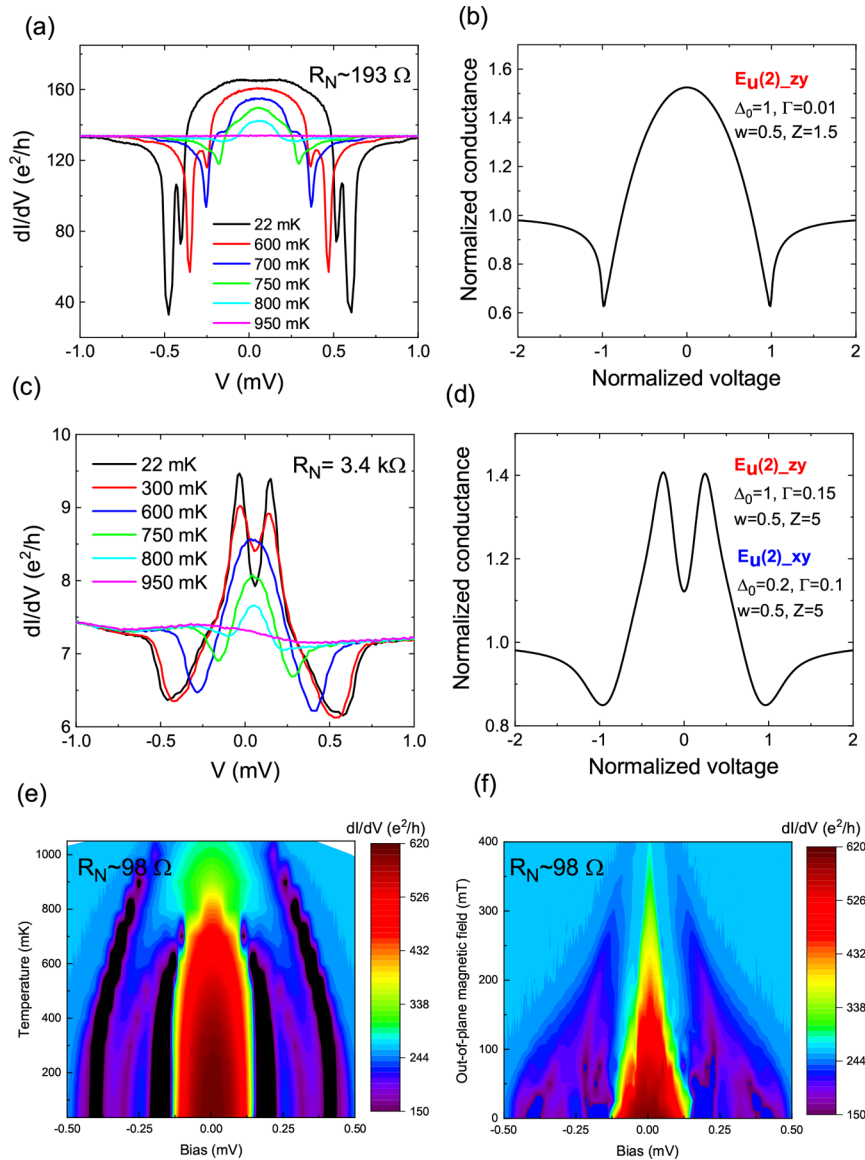


Figure 3. (a) Measured Andreev reflection spectra at various temperatures for a low resistance device with $R_N = 193$ ohms. (b) Simulated spectrum for (a) at the lowest temperature with a single gap. (c,d) Measured and calculated spectra (at the lowest temperature) for a high resistance device with $R_N = 3.4$ kohms. In (b,d), voltage is normalized by the superconducting energy gap and conductance is normalized by the normal state conductance, R_N . Temperature (e) and magnetic field (f) dependence of conductance spectra from another device with transparent contacts. Zero bias conductance peaks gradually get weaker with both temperature and magnetic field.

polarizations emerge in $\text{Nb}_x\text{Bi}_2\text{Se}_3$. In addition, new Fermi surfaces seem to develop upon Nb doping. As we will argue below, such band structure leads to novel features of superconducting state.

Here, we report anomalous Andreev reflection spectra from $\text{Au}/\text{Nb}_x\text{Bi}_2\text{Se}_3$ junctions with varying transparencies that are inconsistent with conventional Blonder–Tinkham–Klapwijk theory for *s*-wave superconductivity.²⁷ These features, including zero bias conductance peaks and dips at the superconducting pairing energy, can be described by certain forms of *p*-wave superconductivity.

Figure 2a shows a scanning electron microscopy (SEM) image of one of the measured devices with two Au localized contacts on top of a 16 nm thick exfoliated thin flake of $\text{Nb}_{0.28}\text{Bi}_2\text{Se}_3$ (data are shown in Figure 3e and f). The bulk samples show robust superconductivity with a transition temperature of 3.5 K.¹⁰ The method by which high quality

samples were grown is discussed elsewhere.¹⁰ Starting with single crystals of $\text{Nb}_{0.28}\text{Bi}_2\text{Se}_3$, we transfer thin flakes onto doped Si substrates with a 300 nm thick oxide layer through the traditional scotch tape method. After thin, flat, and large area pieces are identified with atomic force microscopy, we define the junction leads by e-beam lithography and lift-off of an e-beam evaporated film of 50 nm Au. Prior to metallization, we employ in situ Ar ion-milling of the sample surface to remove any native oxides or other contaminants. The light etching (about a few seconds with a beam current of 10 mA and beam voltage of 400 V) of the crystal surface cleans the NS interface and improves contact resistance. Etching will also produce a rougher surface with multiple crystallographic planes contributing to the NS interface. Incomplete etching will generate NS junctions with thin tunnel barriers with reduced transparency and higher resistances. Although not used in the measurements presented here, a top gate was created by first

depositing a thin layer of Al_2O_3 on the devices via atomic layer deposition. The top gate is defined with a second lithographic process (see Figure 2a), followed by e-beam evaporation of Au. The devices were thermally anchored to the mixing chamber of a cryogen-free dilution refrigerator equipped with a vector magnet and filtered wiring. We perform low-frequency transport measurements with standard lock-in techniques, typically with a 10 nA AC excitation at 73 Hz.

Devices with six contacts in a Hall bar geometry as shown in the inset of Figure 2b allow measurements of intrinsic dissipation R_{xx} while avoiding the influence of contact resistance. The longitudinal resistance versus temperature obtained from a Hall bar device fabricated on a 17 nm thick flake demonstrates a transition temperature of 800 mK as shown in the main panel of Figure 2b. This is significantly reduced from the bulk value due to either finite size effects or disorder.

Devices with only two or three normal metal leads are employed for Andreev reflection spectroscopy of the NS interface. Differential conductance versus voltage, dI/dV versus V , characteristics of a sample with relatively transparent Au/ $\text{Nb}_{0.28}\text{Bi}_2\text{Se}_3$ interface are shown in Figure 3a for various temperatures. Below the critical temperature, the device shows significant enhancement in conductance around zero bias due to Andreev reflection at the interface of $\text{Nb}_{0.28}\text{Bi}_2\text{Se}_3$ and Au followed by additional high bias features. These broad zero bias conductance (ZBC) peaks are accompanied by sharp dips at the superconducting gap, which are not observed in superconductors with conventional s -wave pairing symmetry. In fact, this abrupt suppression of conductance at superconducting gap is a signature of shifting spectral weight away from high energy states to form low energy surface bound states and is often associated with p -wave pairing symmetry.²⁸ We typically observe energy gaps in the range of 100–500 μV . One can notice two sets of conductance dips in Figure 3a. This could be ascribed to two different energy gaps of similar but distinct magnitudes. We will discuss this possibility in greater detail later on.

Despite numerous calculations for the Andreev conductance spectra for the various categories of odd-parity and topological superconductivity (e.g., refs 28–31), determining which pairing symmetry corresponds to an observed conductance spectra is problematic because the presence of multiple fitting parameters permit agreement with more than one model. In Figure 3b, we show calculated conductance spectra of a p -wave symmetry superconductor junction by using the $E_u(2)$ model shown in ref 30 for a moderate barrier strength of $Z = 1.5$ to represent the partial transparency of the NS interface and match the shape of the observed spectrum in Figure 3a. We include a broadening parameter Γ to reflect inelastic scattering or thermal fluctuations and a weighting parameter w to match the height of the conductance peak relative to the background conductance. For $E_u(2)$ symmetry, the matrix form of the pair potential, Δ , can be written in terms of polar and azimuthal angles θ and ϕ where $\Delta_{\uparrow\uparrow}(\theta, \phi) = \Delta_0 e^{i\phi} \sin \theta$ and $\Delta_{\uparrow\downarrow}(\theta, \phi) = \Delta_{\downarrow\uparrow}(\theta, \phi) = \Delta_{\downarrow\downarrow}(\theta, \phi) = 0$. In that model, tunneling in the z - y plane gives a prominent ZBC peak, as do several other odd-parity models in other directions. Because of the surface roughness induced by ion milling prior to deposition of the gold leads, it is likely that our devices include contributions from tunneling into both the z - y and the x - y planes of the $\text{Nb}_x\text{Bi}_2\text{Se}_3$ crystal. We do not presume $E_u(2)$ is the actual pairing symmetry of $\text{Nb}_{0.28}\text{Bi}_2\text{Se}_3$, but we select it for our

modeling because other experimental studies are also consistent with this pairing symmetry^{22,23} and to show its agreement with our results. Although material-specific conditions such as interorbital interactions might alter the exact structure of the pairing interaction,^{20,21} it is probable that our simple formalism for the pairing should be sufficient to qualitatively describe our experimental results.

Having discussed the devices with relatively more transparent NS contacts, we now turn to conductance spectra of comparatively higher contact resistance devices. Such devices typically demonstrate a split peak at low temperatures instead of a single broad ZBC peak due to increasing barrier strength at the NS interface.²⁷ Figure 3c shows temperature dependence of differential conductance characteristics from a device with the normal state resistance R_N of 3.4 k Ω . The well-defined split peak feature accompanied by a sharp dip at the superconducting gap at low temperatures gets suppressed with temperature and eventually evolves into a single peak around zero bias beyond 600 mK. Above 950 mK, superconductivity is completely lost.

We plot a simulated spectrum in Figure 3d using the $E_u(2)$ model with a large barrier strength of $Z = 5$. To capture the split peak feature of Figure 3c, we include contributions from tunneling into both the z - y plane (with normalized pairing energy $\Delta_0 = 1$) and the x - y plane (with a smaller pairing energy $\Delta_0 = 0.2$).

We also note that the split peak shape in Figure 3c can result from surface Andreev bound states.^{9,13} Such subgap states form on the surface of topological superconductors and lead to a characteristic split peak feature in spectroscopic measurements due to van Hove singularities in their density of states.¹³ A caveat is that refs 9 and 13 considered the case of time-reversal symmetric topological superconductors, although it is possible that similar features are observable in topological superconductors with broken time-reversal symmetry such as $\text{Nb}_x\text{Bi}_2\text{Se}_3$.

Although a finite critical current might also generate spurious ZBC peaks,³² strong temperature and magnetic field dependence of the conductance at zero voltage can help to rule this out. To investigate this, we show color plots of dI/dV versus V as a function of temperature and magnetic field from another low contact resistance-Andreev reflection device made with 16 nm thick flake in Figures 3e,f. We observe that above 300 mK the height of the zero bias conductance continually drops as temperature increases as shown in Figure 3e. Similarly, conductance at zero bias also decreases in the presence of a small magnetic field (Figure 3f) despite the persistence of strong coherence dips. As argued by ref 9, this behavior is incompatible with false zero bias conductance peaks generated by finite critical current, which would leave zero bias conductance unchanged after small rises in temperature or magnetic field. Instead, the apparent width of the zero bias conductance peak would shrink due to the reduction in the critical current. Further discussion can be found in the Supporting Information.

Furthermore, one can see the coherent conductance dips just beyond the superconducting gaps in high resistance samples as observed in devices with more transparent contacts. The appearance of such conductance dips in high resistance samples helps to rule out finite critical currents as the source of the anomalous suppression in conductance at the superconducting energy gap.

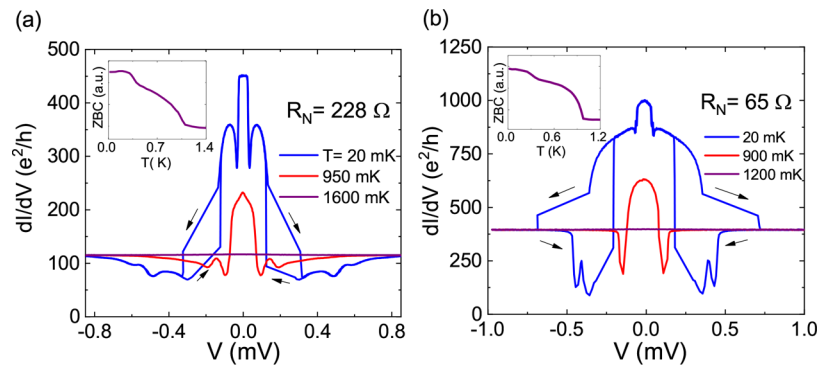


Figure 4. (a,b) Andreev spectra from two different devices that each contain two apparently different energy gaps. Hysteretic current–voltage behavior leads to discontinuities in the measured spectra. The sweep direction of the bias current is indicated by the arrows.

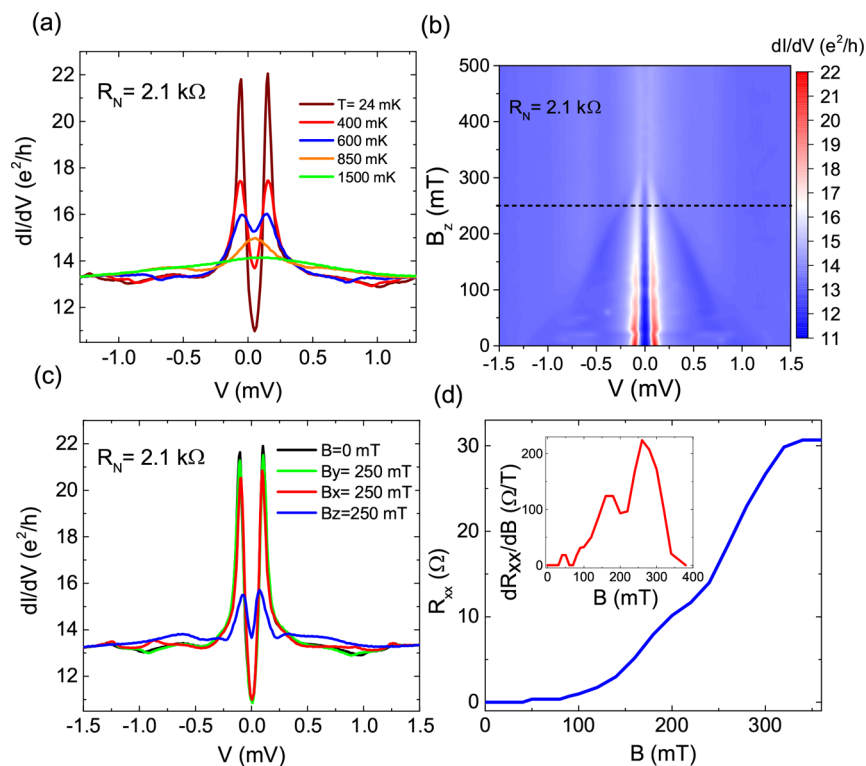


Figure 5. (a) Temperature dependence of differential conductance of one of the high resistance devices. (b) Color plot of out of magnetic field dependence of dI/dV for the same device. (c) Comparison of in-plane and out-of-plane magnetic field dependence of differential conductance, showing a strong directional anisotropy. (d) Longitudinal resistance as a function of out-of-plane magnetic field obtained from a Hall bar device.

One can compare our results with previous spectroscopic studies of NbSe_2 .^{33,34} Like Nb-doped Bi_2Se_3 , NbSe_2 can be exfoliated to produce thin flakes. However, it is thought to be an *s*-wave superconductor. In particular, one study³³ reported the conductance spectra of NbSe_2 /graphene junction where the interface transparency can be varied by gating the graphene. Thus, the NS junction can be in situ tuned between the tunneling and Andreev reflection regimes. In contrast to our results, their obtained spectra in all regimes lack of coherence dips at the superconducting gap and are able to be described by the standard BTK model employing superconductors with isotropic homogeneous gap.

Now, we return to the possibility for multigap superconductivity with a different batch of crystals showing much clearer additional conductance features at the lowest temperatures. In Figure 4a,b, the 20 mK conductance traces exhibit a robust additional ZBC peak that is superimposed on the

broader main ZBC peak. Like the main broad Andreev reflection feature, this additional conductance peak is accompanied by strong dips in conductance. At the low temperatures, the observed I – V characteristics are highly hysteretic, possibly due to a circuit instability caused by a large negative differential conductance³⁵ or by heating; in any event, the coherence dips associated with the main Andreev reflection features are partially obscured at 20 mK traces. The arrows in 20 mK traces show the direction in which we sweep the bias current. As the temperature is increased but still below T_c , these dips are clearly observed in spectra (see the conductance spectra for each sample in red). The insets show the temperature dependence of the zero bias conductance versus temperature in which two distinct transitions are apparent. The additional Andreev reflection features disappear roughly around 300 mK and suggest the presence of an extra smaller gap closing at lower temperatures.

Such additional features appearing at low temperatures and low energies could be due to the multiple Fermi surfaces of $\text{Nb}_x\text{Bi}_2\text{Se}_3$, as also observed in other exotic materials with complex pairing such as Sr_2RuO_4 .³⁶ As argued above, our calculated band structures of Nb intercalated Bi_2Se_3 slabs show that Nb states hybridize with host Bi_2Se_3 states near the Fermi level resulting in multiple spin-dependent Fermi surfaces.²⁶ Superconducting pairing in such a band structure (pairing within the bands or between various bands) could yield our experimental observations of Andreev conductance spectra with multiple gap features.

The additional features at low energy can also result from spatial inhomogeneity of the superconducting gap in the NS devices. For example, there might be regions of weakened superconductivity in the $\text{Nb}_{0.28}\text{Bi}_2\text{Se}_3$ crystals, such as in the regions directly in contact with the gold probe, which could exhibit a smaller superconducting gap from an inverse proximity effect.³⁷ On the other hand, the inverse proximity effect is expected to result in a smoothly varying gap in the superconductor near the NS interface. It is not clear to us how the inverse proximity effect might create a single, distinctly smaller gap observed through spectroscopy.

We finally discuss the magnetotransport properties of our devices. We first consider another high resistance Andreev reflection device with $R_N = 2.1 \text{ k}\Omega$ whose temperature-dependent conductance spectra at zero field is shown in Figure 5a. Similar to the device shown in Figure 3c, here we also observe a split peak centered on zero bias with depressed conductance at finite bias. We plot the evolution of the Andreev spectrum of the device with out of plane magnetic field, B_z , in Figure 5b. Curiously, the location of the two peaks remain essentially independent of magnetic field. Faint signatures of the two peaks remain even after the magnetic field has fully quenched other features of Andreev reflection. We do not observe a splitting of the peaks with magnetic field, helping to rule out a Kondo effect³⁸ or other types magnetic anomalies as an origin for the zero bias conductance peaks.

The magnetotransport measurements of three-dimensional (3D) bulk crystals of the Nb-doped Bi_2Se_3 have been reported to show strong directional anisotropy.²² Thus, we explore the magnetic field direction anisotropy on conductance characteristics on thin flakes. Figure 5c shows differential conductance traces of the same high resistance sample at 250 mT as the magnetic field is applied in-plane (B_x or B_y) and out-of-plane (B_z) orientations with respect to the substrate. The blue curve is the single conductance trace with perpendicular magnetic field marked with dashed lines in Figure 5b. The conductance spectra are highly affected by the out-of-plane magnetic field but remain almost unchanged with the in-plane magnetic field. All spectral features are suppressed beyond 300 mT with out-of-plane magnetic field as seen in Figure 5b. This suggests that there is a strong anisotropy of critical field between in-plane and out-of-plane directions. Thus, our thin flakes are in a quasi two-dimensional limit, in which orbital effects are determined by mostly in-plane motion rather than out-of-plane motion. It is not yet clear whether this reduced dimensionality arises from the extreme thinness of our devices compared to the superconducting coherence length or reflects the dominance of two-dimensional surface states.

Figure 5d shows longitudinal resistance as a function of out-of-plane magnetic field obtained from the same Hall bar device in Figure 2b that is constructed from a 17 nm thick flake. Prior to reaching the upper critical magnetic field, we observe finite

resistance, suggesting the dissipative flow of magnetic vortices.³⁹ The resistance begins to rise most dramatically beyond 100 mT, which we tentatively identify as the lower critical field for this particular thin flake. One can observe at least two distinct transitions with the magnetic field, which are absent in the temperature dependence of resistance shown in Figure 2b. The derivation of R_{xx} with respect to magnetic field in the insets of Figure 5d gives three peaks corresponding to these transitions. These multiple critical fields suggest the formation of different vortex states.⁴⁰ Our results suggest the feasibility of introducing magnetic vortices in Nb-doped Bi_2Se_3 , which could potentially harbor zero-energy Majorana bound states.^{41,42}

In summary, we explored the differential conductance spectroscopy of exfoliated thin pieces of Nb-doped Bi_2Se_3 coupled to normal metal leads at different spectral regimes. We observed an upper critical field anisotropy between in-plane and out-of-plane directions suggesting the $\text{Nb}_{0.28}\text{Bi}_2\text{Se}_3$ flakes are in the two-dimensional limit. At low temperatures, we observed a broad enhancement in conductance at low energies, consistent with Andreev reflection. However, the enhanced conductance persists even in high resistance devices and is accompanied by coherence dips at the superconducting gap that are not explained by conventional BTK theory and are associated with p -wave symmetry pairing. Most of the obtained conductance spectra show multiple gap features originating from unconventional band structure of $\text{Nb}_x\text{Bi}_2\text{Se}_3$ and the presence of additional Fermi surfaces. Our results advance the understanding of topological superconductivity in doped topological insulators and motivate other studies in the field of three-dimensional topological superconductors.

■ ASSOCIATED CONTENT

📄 Supporting Information

The Supporting Information is available free of charge on the ACS Publications website at DOI: 10.1021/acs.nanolett.8b02954.

Further discussion on the nature of observed zero bias conductance peaks as well as the electronic band calculations of Nb-intercalated Bi_2Se_3 slab (PDF)

■ AUTHOR INFORMATION

Corresponding Author

*E-mail: kurterc@mst.edu.

ORCID

C. Kurter: 0000-0002-1867-9213

Present Address

¹(A.D.K.F.) IBM Thomas J. Watson Research Center, Yorktown Heights, New York 10598, United States

Notes

The authors declare no competing financial interest.

■ ACKNOWLEDGMENTS

C.K., A.D.K.F., E.D.H., and D.J.V.H. would like to acknowledge funding by Microsoft Station-Q. E.D.H. and D.J.V.H. acknowledge funding from the NSF Grant DMR 17-10437. T.V. acknowledges funding from the NSF Grant DMR-1506152. P.G. acknowledges support from the NSF CREST Center for Interface Design and Engineered Assembly of Low Dimensional systems (IDEALS) and the NSF Grant HRD-1547830. Y.S.H. acknowledges funding from the NSF Grant

DMR-1255607. J.E.M. acknowledges the computational support provided by XSEDE and NERSC. For the device fabrication, we acknowledge the use of the facilities of the Frederick Seitz Materials Research Laboratory at the University of Illinois at Urbana–Champaign, supported by the Department of Energy. We would like to thank Jessica Terbush for assistance of imaging the samples. We are thankful for helpful discussions with Fan Zhang.

REFERENCES

- (1) Sacépé, B.; Oostinga, J. B.; Li, J.; Ubal dini, A.; Couto, N. J.; Giannini, E.; Morpurgo, A. F. Gate-tuned normal and superconducting transport at the surface of a topological insulator. *Nat. Commun.* **2011**, *2*, 575.
- (2) Williams, J. R.; Bestwick, A. J.; Gallagher, P.; Hong, S. S.; Cui, Y.; Bleich, A. S.; Analytis, J. G.; Fisher, I. R.; Goldhaber-Gordon, D. Unconventional Josephson Effect in Hybrid Superconductor-Topological Insulator Devices. *Phys. Rev. Lett.* **2012**, *109*, 056803.
- (3) Veldhorst, M.; Snelder, M.; Hoek, M.; Gang, T.; Guduru, V. K.; Wang, X. L.; Zeitler, U.; van der Wiel, W. G.; Golubov, A. A.; Hilgenkamp, H.; Brinkman, A. Josephson supercurrent through a topological insulator surface state. *Nat. Mater.* **2012**, *11*, 417.
- (4) Cho, S.; Dellabetta, B.; Yang, A.; Schneeloch, J.; Xu, Z.; Valla, T.; Gu, G.; Gilbert, M. J.; Mason, N. Symmetry protected Josephson supercurrents in three-dimensional topological insulators. *Nat. Commun.* **2013**, *4*, 1689.
- (5) Kurter, C.; Finck, A. D. K.; Ghaemi, P.; Hor, Y. S.; Van Harlingen, D. J. Dynamical gate-tunable supercurrents in topological Josephson junctions. *Phys. Rev. B: Condens. Matter Mater. Phys.* **2014**, *90*, 014501.
- (6) Stehno, M. P.; Orlyanchik, V.; Nugroho, C. D.; Ghaemi, P.; Brahlek, M.; Koirala, N.; Oh, S.; Van Harlingen, D. J. Signature of a topological phase transition in the Josephson supercurrent through a topological insulator. *Phys. Rev. B: Condens. Matter Mater. Phys.* **2016**, *93*, 035307.
- (7) Kurter, C.; Finck, A. D. K.; Hor, Y. S.; Van Harlingen, D. J. Evidence for an anomalous current-phase relation in topological insulator Josephson junctions. *Nat. Commun.* **2015**, *6*, 7130.
- (8) Hor, Y. S.; Williams, A. J.; Checkelsky, J. G.; Roushan, P.; Seo, J.; Xu, Q.; Zandbergen, H. W.; Yazdani, A.; Ong, N. P.; Cava, R. J. Superconductivity in $\text{Cu}_x\text{Bi}_2\text{Se}_3$ and its Implications for Pairing in the Undoped Topological Insulator. *Phys. Rev. Lett.* **2010**, *104*, 057001.
- (9) Sasaki, S.; Kriener, M.; Segawa, K.; Yada, K.; Tanaka, Y.; Sato, M.; Ando, Y. Topological Superconductivity in $\text{Cu}_x\text{Bi}_2\text{Se}_3$. *Phys. Rev. Lett.* **2011**, *107*, 217001.
- (10) Qiu, Y.; Sanders, K. N.; Dai, J.; Medvedeva, J. E.; Wu, W.; Ghaemi, P.; Vojta, T.; Hor, Y. S. Time reversal symmetry breaking superconductivity in topological materials. **2016**, arXiv:1512.03519 (accessed Oct 2018).
- (11) Liu, Z.; Yao, X.; Shao, J.; Zuo, M.; Pi, L.; Tan, S.; Zhang, C.; Zhang, Y. Superconductivity with Topological Surface State in $\text{Sr}_x\text{Bi}_2\text{Se}_3$. *J. Am. Chem. Soc.* **2015**, *137*, 10512–10515.
- (12) Peng, H.; De, D.; Lv, B.; Wei, F.; Chu, C.-W. Absence of zero-energy surface bound states in $\text{Cu}_x\text{Bi}_2\text{Se}_3$ studied via Andreev reflection spectroscopy. *Phys. Rev. B: Condens. Matter Mater. Phys.* **2013**, *88*, 024515.
- (13) Hsieh, T. H.; Fu, L. Majorana Fermions and Exotic Surface Andreev Bound States in Topological Superconductors: Application to $\text{Cu}_x\text{Bi}_2\text{Se}_3$. *Phys. Rev. Lett.* **2012**, *108*, 107005.
- (14) Majorana, E. A symmetric theory of electrons and positrons. *Nuovo Cimento* **1937**, *14*, 171.
- (15) Wilczek, F. Majorana returns. *Nat. Phys.* **2009**, *5*, 614.
- (16) Nayak, C.; Simon, S. H.; Stern, A.; Freedman, M.; Das Sarma, S. Non-Abelian anyons and topological quantum computation. *Rev. Mod. Phys.* **2008**, *80*, 1083–1159.
- (17) Tinkham, M. *Introduction to Superconductivity*; Dover Publications, Inc., 1996.
- (18) Levy, N.; Zhang, T.; Ha, J.; Sharifi, F.; Talin, A. A.; Kuk, Y.; Stroscio, J. A. Experimental Evidence for s-Wave Pairing Symmetry in Superconducting $\text{Cu}_x\text{Bi}_2\text{Se}_3$ Single Crystals Using a Scanning Tunneling Microscope. *Phys. Rev. Lett.* **2013**, *110*, 117001.
- (19) Matano, K.; Kriener, M.; Segawa, K.; Ando, Y.; Zheng, G. Spin-rotation symmetry breaking in the superconducting state of $\text{Cu}_x\text{Bi}_2\text{Se}_3$. *Nat. Phys.* **2016**, *12*, 852.
- (20) Chirrolli, L.; de Juan, F.; Guinea, F. Time-reversal and rotation symmetry breaking superconductivity in Dirac materials. *Phys. Rev. B: Condens. Matter Mater. Phys.* **2017**, *95*, 201110.
- (21) Yuan, N. F. Q.; He, W.-Y.; Law, K. T. Superconductivity-induced ferromagnetism and Weyl superconductivity in Nb-doped Bi_2Se_3 . *Phys. Rev. B: Condens. Matter Mater. Phys.* **2017**, *95*, 201109.
- (22) Asaba, T.; Lawson, B. J.; Tinsman, C.; Chen, L.; Corbae, P.; Li, G.; Qiu, Y.; Hor, Y. S.; Fu, L.; Li, L. Rotational Symmetry Breaking in a Trigonal Superconductor Nb-doped Bi_2Se_3 . *Phys. Rev. X* **2017**, *7*, 011009.
- (23) Smylie, M. P.; Claus, H.; Welp, U.; Kwok, W.-K.; Qiu, Y.; Hor, Y. S.; Snezhko, A. Evidence of nodes in the order parameter of the superconducting doped topological insulator $\text{Nb}_x\text{Bi}_2\text{Se}_3$ via penetration depth measurements. *Phys. Rev. B: Condens. Matter Mater. Phys.* **2016**, *94*, 180510.
- (24) Wilfert, S.; Sessi, P.; Wang, Z.; Schmidt, H.; Martínez-Velarte, M. C.; Lee, S. H.; Hor, Y. S.; Otte, A. F.; Ando, Y.; Wu, W.; Bode, M. Scanning tunneling spectroscopy investigations of superconducting-doped topological insulators: Experimental pitfalls and results. *Phys. Rev. B: Condens. Matter Mater. Phys.* **2018**, *98*, 085133.
- (25) Sirohi, A.; Das, S.; Neha, P.; Jat, K. S.; Patnaik, S.; Sheet, G. Low-energy excitations and non-BCS superconductivity in $\text{NbxBi}_2\text{Se}_3$. *Phys. Rev. B: Condens. Matter Mater. Phys.* **2018**, DOI: 10.1103/PhysRevB.98.094523
- (26) Lawson, B. J.; Corbae, P.; Li, G.; Yu, F.; Asaba, T.; Tinsman, C.; Qiu, Y.; Medvedeva, J. E.; Hor, Y. S.; Li, L. Multiple Fermi surfaces in superconducting Nb-doped Bi_2Se_3 . *Phys. Rev. B: Condens. Matter Mater. Phys.* **2016**, *94*, 041114.
- (27) Blonder, G. E.; Tinkham, M.; Klapwijk, T. M. Transition from metallic to tunneling regimes in superconducting microconstrictions: Excess current, charge imbalance, and supercurrent conversion. *Phys. Rev. B: Condens. Matter Mater. Phys.* **1982**, *25*, 4515–4532.
- (28) Yamakage, A.; Yada, K.; Sato, M.; Tanaka, Y. Theory of tunneling conductance and surface-state transition in superconducting topological insulators. *Phys. Rev. B: Condens. Matter Mater. Phys.* **2012**, *85*, 180509.
- (29) Yamashiro, M.; Tanaka, Y.; Kashiwaya, S. Theory of tunneling spectroscopy in superconducting Sr_2RuO_4 . *Phys. Rev. B: Condens. Matter Mater. Phys.* **1997**, *56*, 7847–7850.
- (30) Yamashiro, M.; Tanaka, Y.; Tanuma, Y.; Kashiwaya, S. Theory of Tunneling Conductance for Normal Metal/Insulator/Triplet Superconductor Junction. *J. Phys. Soc. Jpn.* **1998**, *67*, 3224–3233.
- (31) Burset, P.; Lu, B.; Tkachov, G.; Tanaka, Y.; Hankiewicz, E. M.; Trauzettel, B. Superconducting proximity effect in three-dimensional topological insulators in the presence of a magnetic field. *Phys. Rev. B: Condens. Matter Mater. Phys.* **2015**, *92*, 205424.
- (32) Sheet, G.; Mukhopadhyay, S.; Raychaudhuri, P. Role of critical current on the point-contact Andreev reflection spectra between a normal metal and a superconductor. *Phys. Rev. B: Condens. Matter Mater. Phys.* **2004**, *69*, 134507.
- (33) Han, T.; Shen, J.; Yuan, N. F. Q.; Lin, J.; Wu, Z.; Wu, Y.; Xu, S.; An, L.; Long, G.; Wang, Y.; Lortz, R.; Wang, N. Investigation of the two-gap superconductivity in a few-layer NbSe_2 -graphene heterojunction. *Phys. Rev. B: Condens. Matter Mater. Phys.* **2018**, *97*, 060505.
- (34) Sahu, M. R.; Raychaudhuri, P.; Das, A. Andreev reflection near the Dirac point at the graphene- NbSe_2 junction. *Phys. Rev. B: Condens. Matter Mater. Phys.* **2016**, *94*, 235451.
- (35) Nandi, D.; Khaire, T.; Finck, A. D. K.; Eisenstein, J. P.; Pfeiffer, L. N.; West, K. W. Tunneling at $\nu_T=1$ in quantum Hall bilayers. *Phys. Rev. B: Condens. Matter Mater. Phys.* **2013**, *88*, 165308.
- (36) Kashiwaya, S.; Kashiwaya, H.; Kambara, H.; Furuta, T.; Yaguchi, H.; Tanaka, Y.; Maeno, Y. Edge States of Sr_2RuO_4 Detected

by In-Plane Tunneling Spectroscopy. *Phys. Rev. Lett.* **2011**, *107*, 077003.

(37) Cherkez, V.; Cuevas, J. C.; Brun, C.; Cren, T.; Ménard, G.; Debontridder, F.; Stolyarov, V. S.; Roditchev, D. Proximity Effect between Two Superconductors Spatially Resolved by Scanning Tunneling Spectroscopy. *Phys. Rev. X* **2014**, *4*, 011033.

(38) Goldhaber-Gordon, D.; Shtrikman, H.; Mahalu, D.; Abusch-Magder, D.; Meirav, U.; Kastner, M. A. Kondo effect in a single-electron transistor. *Nature* **1998**, *391*, 156–159.

(39) Kim, Y. B.; Hempstead, C. F.; Strnad, A. R. Flux-Flow Resistance in Type-II Superconductors. *Phys. Rev.* **1965**, *139*, A1163–A1172.

(40) Geim, A. K.; Grigorieva, I. V.; Dubonos, S. V.; Lok, J. G. S.; Maan, J. C.; Filippov, A. E.; Peeters, F. M. Phase transitions in individual sub-micrometre superconductors. *Nature* **1997**, *390*, 259.

(41) Fu, L.; Kane, C. L. Superconducting Proximity Effect and Majorana Fermions at the Surface of a Topological Insulator. *Phys. Rev. Lett.* **2008**, *100*, 096407.

(42) Hosur, P.; Ghaemi, P.; Mong, R. S. K.; Vishwanath, A. Majorana modes at the ends of superconductor vortices in doped topological insulators. *Phys. Rev. Lett.* **2011**, *107*, 097001.